Maneuvering Target Tracking: A Gaussian Mixture Based IMM Estimator

Dann Laneuville
DCNS Research
40-42, Rue du Docteur Finlay
75732 Paris cedex 15, France
dann.laneuville@dcnsgroup.com

Yaakov Bar-Shalom
University of Connecticut
260 Glenbrook Road, U-157
Storrs, CT 06269
ybs@engr.uconn.edu

Abstract— **This paper[1,2] revisits the problem of maneuvering target tracking and presents a new algorithm to circumvent the exponential growth of the hypotheses (mixture elements) that arises in the optimal multiple model filter. The idea of the new scheme is to replace this increasing burden at each step by a Gaussian mixture, thus maintaining a limited number of hypotheses in the filter. Numerous comparative simulations with the IMM, both in active and passive measurement cases, show that this new approach improves significantly the tracking performance in the passive case. In the active case, on the contrary, the IMM seems to remain the best complexity-performance compromise.**

TABLE OF CONTENTS

1. INTRODUCTION

Since the original work on the Interacting Multiple Model (IMM) estimator in [2], many papers have successfully used this algorithm for maneuvering target tracking problems in different contexts. This paper revisits the problem of maneuvering target tracking and presents a new algorithm. The idea, used to circumvent the exponential number of hypotheses that arises in the optimal multiple model filter, is to replace them at each step by a Gaussian Mixture (GM) in each mode, thus maintaining a limited number of hypotheses. The new algorithm is designated as Gaussian Mixture Interacting Multiple Model (GMIMM) estimator.

The paper is organized as follows. In Section 2 we review the IMM estimator. Section 3 describes the new algorithm. We present simulation results in Section 4 from both passive and active measurement cases, with two sub cases in the passive case: a Bearing Only Tracking (BOT) application and a bearing and Doppler application. The performance of the GMIMM is also compared with the conventional IMM estimator in terms of Root Mean Square (RMS) error in position, velocity and computational requirements. Finally, we give some concluding remarks.

2. REWIEW OF THE IMM ESTIMATOR

As it is highly desirable in a maneuvering target tracking context, we use the *switching* multiple models description [3] to derive our new scheme. In this context, the target dynamics are described by

- a finite collection of m models, each one corresponding to a possible state evolution (system mode),
- and a Markov chain to describe the jumps between the different models.

Assume the target dynamics can jump from one model to another during the tracking process and denote by $M(k) \in \{1, \cdots, m\}$ the model in effect between time t_k and t_{k+1}. The mode transitions are modeled by the Markov chain with Probability Transition Matrix (PTM)

$$p_{ij} = P(M(k+1) = j \,|\, M(k) = i) \tag{2.1}$$

Let $x(k)$ and $z(k)$ be respectively the state vector and the measurement at time k. Then, we have

$$\begin{cases} x(k+1) = f(M(k), x(k)) + v(k, M(k)) \\ z(k) = h(M(k), x(k)) + w(k, M(k)) \end{cases} \tag{2.2}$$

with $f(M(k), x(k))$ the prediction step corresponding to the current model, i.e. the model in effect between time t_k and t_{k+1}, $v(k, M(k))$ the process noise assumed to be zero-mean and normally distributed with covariance $Q(M(k))$. $h(M(k), x(k))$ is the measurement function and $w(k, M(k))$ the measurement noise also assumed to be zero-mean and normally distributed with covariance $R(M(k))$.

To clearly understand why the optimal filter requires ever increasing memory, even with linear dynamics in (2.2), and thus needs to be approximated, consider Fig.1 which represents the mode evolution history denoted as $\{M^{k,n}\}$, with $n = m^{k+1}$ possible paths at time k (because we start with $k = 0$). Each line can be seen as the propagation

[1] Proc. 2012 IEEE/AIAA Aerospace Conf., Big Sky, MT, March 2012

[2] Research of YBS sponsored under ONR N00014-07-1-0131 and ARO W911NF-06-1-0467 grants.

978-1-4577-0557-1/12/$26.00 ©2012 IEEE

Authorized licensed use limited to: Purdue University. Downloaded on September 15,2025 at 23:34:05 UTC from IEEE Xplore. Restrictions apply.

(prediction and update) between time t_k and t_{k+1} of a Gaussian density by the mode-matched filters. With linear dynamics in (2.2), this is optimally achieved by a Kalman filter, otherwise an EKF, Unscented Kalman Filter (UKF) or Particle Filter (PF) can be used. See for example respectively [3], [5] and [1] for those alternatives.

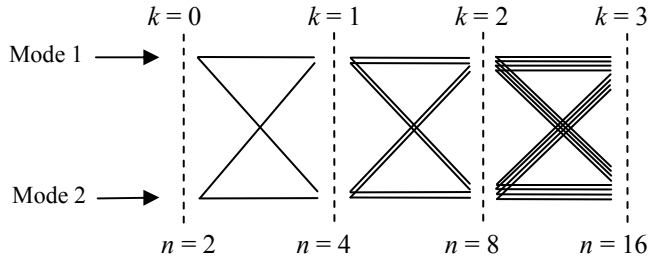

Fig.1 – Hypotheses history $\{M^{k,n}\}$ for $m = 2$ modes

The conditional density of the state at time k is obtained by using the total probability theorem with respect to the set of the n possible modal evolution paths at time k, and is a Gaussian mixture with an exponentially increasing number of terms [3], namely,

$$p(x(k)|Z^k) = \sum_{n=1}^{m^{k+1}} p(x(k)|M^{k,n}, Z^k) P\left\{M^{k,n}\middle|Z^k\right\} \tag{2.3}$$

Thus, some approximations are needed to obtain implementable solutions. The IMM consists, for a given mode, in merging different hypothesis at the beginning of a cycle into a single hypothesis which represents the new initial estimate to be propagated under the mode-matched filter in the following cycle.

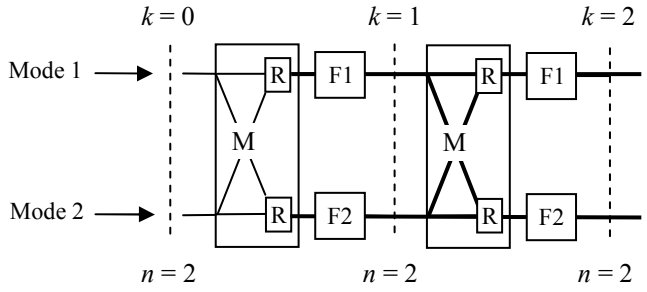

Fig.2 – IMM for $m = 2$ modes. Square blocks perform filtering, rectangular blocks mixing and reduction

3. GMIMM DESCRIPTION

The merging approach discussed above is generally preferred to the other suboptimal class of solutions, the track-splitting and pruning approach. It has been indeed reported that this solution, where unlikely mode sequences are discarded, can produce a divergent track by eliminating a valid sequence after a maneuver.

We present here a new scheme which limits the summation in (2.3). The idea of this new approach consists of maintaining constant the number of mixture terms for each mode. More precisely, at the end of each mixing, the number of terms of the GM in each mode, namely $(r+1) \times m$, is reduced and kept constant by choosing for the GM the r most probable hypotheses. The remaining hypotheses are merged into a single one and will complete the GM which now contains $r+1$ terms for each mode. Then, at the beginning of the filtering cycle and for each mode, the $r+1$ terms are propagated via the current mode-matched filter leading to a set of $(r+1)$ hypotheses in each mode for the beginning of the next cycle and so on. Thus, there are a total $n = (r+1) \times m$ terms in the Gaussian mixture (2.3) while there are only m in the conventional IMM scheme. To clearly understand the structure of the filter with the reduction phase of the $(r+1) \times m$ mixture elements into $r+1$ terms (represented by a block with letter R) at each mode and at the beginning of a new cycle, Fig.3 below illustrates the new scheme with $r = 1$ (which is certainly a good compromise as discussed below) where thick lines represent the merged hypotheses. Contrary to the IMM estimator, the reduction begins, in this case, at the beginning of the second iteration.

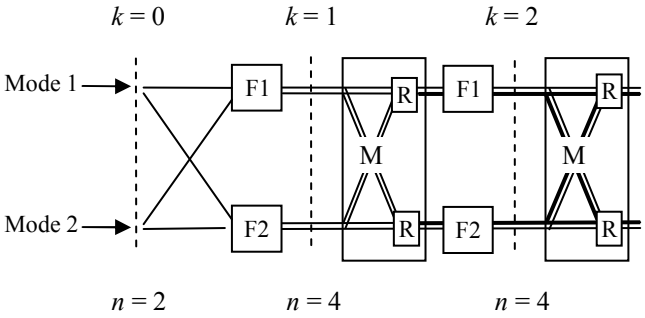

Fig.3 – GMIMM for $m = 2$ modes and $r = 1$. Square blocks perform filtering, rectangular blocks mixing and reduction

Note that until $m^k \le r$, this new approach represents the exact and optimal filter in the linear dynamic case. Also note that a single density is propagated in each mode for the IMM, thus m densities have to be propagated, or equivalently m filters have to be run, while the GMIMM needs to propagate $r+1$ densities for each mode and thus a total of $(r+1) \times m$ densities have to be propagated at each cycle. This can be summarized by the structure of the algorithm, which is

$$\left(N_e, N_f\right) = \left((r+1)m, (r+1)m\right) \tag{3.1}$$

where N_e is the number of estimates at the beginning of a cycle and is N_f the number of filters to be run. In comparison, the structure of the IMM is

$$\left(N_e, N_f\right) = \left(m, m\right) \tag{3.2}$$

and the one of the Generalized Pseudo-Bayes filter of order 2 (GPB_2) is

$$\left(N_e, N_f\right) = \left(m, m^2\right) \tag{3.3}$$

Note that for $r = 0$, the structure of our approach is the same as the IMM. Next we describe in detail the proposed

Authorized licensed use limited to: Purdue University. Downloaded on September 15,2025 at 23:34:05 UTC from IEEE Xplore. Restrictions apply.

GMIMM algorithm for m modes and the r most likely hypotheses to be kept in each mode, with the remainder being combined into a single hypothesis.

GMIMM algorithm, m modes, $r+1$ mixture elements per mode

Filter Initialization: $k = 0$

The state vectors are initialized in each mode j with a prior mean $\hat{x}_j(0)$ and a prior covariance matrix $P_j(0)$, as well as a prior probability distribution $\mu_j(0)$, such that

$$\sum_{j=1}^{m} \mu_j(0) = 1 \tag{3.4}$$

exactly like in the IMM.

Input at time $k-1$

At time $k-1$ the input of the algorithm consists of a set of m mixtures of $r+1$ elements (the mixtures start with one element and grow until $r+1$) given by

$$p\left[x(k-1)\middle|Z^{k-1}\right] = \sum_{i=1}^{m}\sum_{l=1}^{r+1} \mu_{i,l}(k-1)\mathcal{N}\left[x(k-1); \hat{x}_{i,l}(k-1|k-1), P_{i,l}(k-1|k-1)\right] \tag{3.5}$$

One cycle of the algorithm consists of the following:

Mixing probabilities

The mixing probabilities for a mixture element at time $k-1$ are calculated as in the conventional IMM

($i, j = 1,\cdots,m$ and $l = 1,\cdots,r+1$)

$$\mu_{i,l|j}(k-1) = \frac{1}{\bar{c}_j} p_{ij}\mu_{i,l}(k-1) \tag{3.6}$$

with the normalizing constants

$$\bar{c}(j) = \sum_{i=1}^{m}\sum_{l=1}^{r+1} p_{ij}\mu_{i,l}(k-1) \qquad j = 1,\cdots,m \tag{3.7}$$

Mixing

The mixing in each mode is done as follows ($j = 1,\cdots,m$)

$$p\left[x(k-1)\middle|M(k)=j, Z^{k-1}\right] = \sum_{i=1}^{m}\sum_{l=1}^{r+1} \mu_{i,l|j}(k-1)\mathcal{N}\left[x(k-1); \hat{x}_{i,l}(k-1|k-1), P_{i,l}(k-1|k-1)\right] \tag{3.8}$$

Reduction of the number of mixture terms

These $(r+1)\times m$ of the above mixture in mode j are reduced to $r+1$ elements by choosing the top r and mixing the remaining ones into a single element according to the standard moment matching equations. The result of the reduction is, ($j = 1,\cdots,m$)

$$p\left[x(k-1)\middle|M(k)=j, Z^{k-1}\right] \approx \sum_{l=1}^{r+1} \mu_{j,l}^{0}(k-1)\mathcal{N}\left[x(k-1); \hat{x}_{j,l}^{0}(k-1|k-1), P_{j,l}^{0}(k-1|k-1)\right] \tag{3.9}$$

Mode-matched filtering

At time k the output of the filter matched to mode j is the GM consisting of $r+1$ elements

$$p\left[x(k)\middle|M(k)=j, Z^{k}\right] = \sum_{l=1}^{r+1} \mu_{j,l}(k)\mathcal{N}\left[x(k); \hat{x}_{j,l}(k|k), P_{j,l}(k|k)\right] \tag{3.10}$$

where the weights $\mu_{j,l}(k)$ follow from the mixture element probability update at the end of cycle k, to be given in the sequel. The mode-matched filtering results are

$$\hat{x}_{j,l}(k|k) = \hat{x}\left[k\middle|k, M(k)=j, \hat{x}(k-1|k-1) = \hat{x}_{j,l}^{0}(k-1|k-1)\right] \tag{3.11}$$

$$P_{j,l}(k|k) = P\left[k\middle|k, M(k)=j, P(k-1|k-1) = P_{j,l}^{0}(k-1|k-1)\right] \tag{3.12}$$

where $\hat{x}_{j,l}^{0}(k-1|k-1)$ and $P_{j,l}^{0}(k-1|k-1)$ are the parameters of the l-th mixture element for mode j, $l = 1,\ldots,r+1$ at the beginning of the cycle k and after the mixing / reduction step.

The likelihood for evaluating the posterior mode probabilities of the l-th mixture element in mode j at time k is

$$\Lambda_{j,l}(k) = p\left[z(k)\middle|M(k)=j, \hat{x}_{j,l}^{0}(k-1|k)\right] = \mathcal{N}\left[z(k); \hat{z}_{j,l}(k|k-1), S_{j,l}(k)\right] \tag{3.13}$$

where

$$\hat{z}_{j,l}(k|k-1) = h\left[M(k), \hat{x}_{j,l}(k|k-1)\right] \tag{3.14}$$

$$\hat{x}_{j,l}(k|k-1) = f\left[M(k), \hat{x}_{j,l}^{0}(k-1|k-1)\right] \tag{3.15}$$

$$S_{j,l}(k) = H\left[M(k), \hat{x}_{j,l}(k|k-1)\right]. P_{j,l}(k|k-1)H\left[M(k), \hat{x}_{j,l}(k|k-1)\right]' + R\left[M(k)\right] \tag{3.16}$$

$$P_{j,l}(k|k-1) = F\left[M(k), \hat{x}_{j,l}(k|k-1)\right]. P_{j,l}^{0}(k-1|k-1)F\left[M(k), \hat{x}_{j,l}(k|k-1)\right]' + Q\left[M(k)\right] \tag{3.17}$$

where H and F are the Jacobians of h and f , respectively.

Authorized licensed use limited to: Purdue University. Downloaded on September 15,2025 at 23:34:05 UTC from IEEE Xplore. Restrictions apply.

Probabilities update

The posterior mode probabilities of the mixture elements at time k are obtained by the following, ($j=1,\cdots,m$ and $l=1,\cdots,r+1$)

$$\mu_{j,l}(k)=\frac{1}{c}\mu^0_{j,l}(k-1)\Lambda_{j,l}(k)\overline{c}_j \tag{3.18}$$

with the normalizing constant

$$c=\sum_{j=1}^{m}\sum_{l=1}^{r+1}\mu^0_{j,l}(k-1)\Lambda_{j,l}(k)\overline{c}_j \tag{3.19}$$

Filter outputs

The filter outputs are, as in the IMM, a weighted combination of the Gaussians in each mode, but here the summation is doubled because we have more than one Gaussian in each mode. The mean value is thus given by

$$\hat{x}(k)=\sum_{j=1}^{m}\sum_{l=1}^{r+1}\mu_{j,l}(k)\hat{x}_{j,l}(k) \tag{3.20}$$

and the covariance by

$$P(k)=\sum_{j=1}^{m}\sum_{l=1}^{r+1}\mu_{j,l}(k)\left[P_{j,l}(k)+\overline{P}_{j,l}(k)\right] \tag{3.21}$$

where $\overline{P}_{j,l}(k)$ is the spread term given by

$$\overline{P}_{j,l}(k)=\left[\hat{x}_{j,l}(k)-\hat{x}(k)\right]\left[\hat{x}_{j,l}(k)-\hat{x}(k)\right]' \tag{3.22}$$

The mode probabilities $\mu_j(k)$ are given by the summation in each mode of the corresponding mixture element probabilities

$$\mu_j(k)=\sum_{l=1}^{r+1}\mu_{j,l}(k) \qquad j=1,\ldots,m \tag{3.23}$$

Note that for $r=0$, we have exactly the conventional IMM equations (in this case, $\mu^0_{j,l}(k-1)\equiv 1$).

Fig.4 in Appendix A presents the block diagram of the GMIMM.

4. SIMULATION RESULTS

We present in this section some results obtained on a 2D scenario with three measurement configurations

- passive with bearing only measurements,
- passive with bearing and Doppler measurements,
- active with bearing and distance measurements.

We describe first the models and measurements which will be used in the simulations. Then we present the scenario and finally some detailed results where we compare the new approach to the IMM filter.

4.1 System modes

Our set of models comprises 2 models: a Nearly Constant Velocity (NCV) model to cover the uniform motion segments and a Nearly Coordinated Turn (NCT) model with *unknown* turn rate ω to cover the maneuvering segments.

State vector and prediction

The state vector is, for the first model,

$$x(k)=\left[\xi(k)\quad \eta(k)\quad \dot{\xi}(k)\quad \dot{\eta}(k)\right]' \tag{3.24}$$

where $\xi(k)$ and $\eta(k)$ are the Cartesian Coordinates (CC) of the target in the 2D plane, and $\dot{\xi}(k)$ and $\dot{\eta}(k)$ the velocity components. The state evolution for the NCV model is

$$x(k+1)=F_1x(k)+v_1(k) \tag{3.25}$$

with

$$F_1=\begin{bmatrix}1&0&T&0\\0&1&0&T\\0&0&1&0\\0&0&0&1\end{bmatrix} \tag{3.26}$$

and $T=t_{k+1}-t_k$, the sampling rate. The NCV model is implemented with the discretized Continuous White Noise Acceleration (CWNA) model ([3]) and the covariance matrix of the process noise is given by

$$Q_1=q_1\begin{bmatrix}T^3/3&0&T^2/2&0\\0&T^3/3&0&T^2/2\\T^2/2&0&T&0\\0&T^2/2&0&T\end{bmatrix} \tag{3.27}$$

where the process noise Power Spectral Density (PSD) $q_1$will be précised in the parameter settings subsection of the Comparative study part. The state vector of model 2 is augmented with the unknown turn rate, namely,

$$x(k)=\left[\xi(k)\quad \eta(k)\quad \dot{\xi}(k)\quad \dot{\eta}(k)\quad \omega(k)\right]' \tag{3.28}$$

The state evolution in mode 2 is here non-linear and is given by

$$x(k+1)=f_2(x(k))+v_2(k) \tag{3.29}$$

Authorized licensed use limited to: Purdue University. Downloaded on September 15,2025 at 23:34:05 UTC from IEEE Xplore. Restrictions apply.

and is approximated up to the second order as

$$f_2(x(k))=\begin{cases}\xi(k)+T\dot{\xi}(k)+\dfrac{T^2}{2}\omega(k)\dot{\eta}(k)\\ \eta(k)+T\dot{\eta}(k)-\dfrac{T^2}{2}\omega(k)\dot{\xi}(k)\\ \dot{\xi}(k)+T\omega(k)\dot{\eta}(k)-\dfrac{T^2}{2}\omega^2(k)\dot{\xi}(k)\\ \dot{\eta}(k)-T\omega(k)\dot{\xi}(k)-\dfrac{T^2}{2}\omega^2(k)\dot{\eta}(k)\\ \omega(k)\end{cases} \tag{3.30}$$

The corresponding process noise covariance matrix is given by

$$Q_2=\begin{bmatrix} q_2\begin{bmatrix} T^3/3 & 0 & T^2/2 & 0\\ 0 & T^3/3 & 0 & T^2/2\\ T^2/2 & 0 & T & 0\\ 0 & T^2/2 & 0 & T\end{bmatrix} & 0_{4\times1}\\ 0_{1\times4} & q_\omega T\end{bmatrix} \tag{3.31}$$

with q_ω the process noise PSD on the turn rate.

Measurements

Our first measurement combination consists of the bearing only and the measurement equation at time *k*,

$$z(k)=\tan^{-1}\left(\frac{\xi(k)-\xi_o(k)}{\eta(k)-\eta_o(k)}\right)+w(k) \tag{3.32}$$

is the same for the two modes with $(\xi_o(k),\eta_o(k))$ denoting the ownship (sensor) location at time *k*, assumed to be perfectly known. The measurement noise covariance matrix is

$$R=\sigma_\beta^2 \tag{3.33}$$

In the case of active measurements, the distance is added to the azimuth angle and (3.32) is replaced by

$$z(k)=\begin{bmatrix}\tan^{-1}\left(\dfrac{\xi(k)-\xi_o(k)}{\eta(k)-\eta_o(k)}\right)\\ \sqrt{(\xi(k)-\xi_o(k))^2+(\eta(k)-\eta_o(k))^2}\end{bmatrix}+w(k) \tag{3.34}$$

and, with σ_d the standard deviation of the measured distance, the covariance matrix is now

$$R=\begin{bmatrix}\sigma_\beta^2 & 0\\ 0 & \sigma_d^2\end{bmatrix} \tag{3.35}$$

In the case of passive measurement with Doppler, the measurement consists in bearing and measured Doppler shift frequency. (3.32) is then replaced by

$$z(k)=\begin{bmatrix}\tan^{-1}\left(\dfrac{\xi(k)-\xi_o(k)}{\eta(k)-\eta_o(k)}\right)\\ f_e(k)\left(1-\dfrac{(\xi-\xi_o)(\dot{\xi}-\dot{\xi}_o)+(\eta-\eta_o)(\dot{\eta}-\dot{\eta}_o)}{c\sqrt{(\xi-\xi_o)^2+(\eta-\eta_o)^2}}\right)\end{bmatrix}+w(k) \tag{3.36}$$

with $f_e(k)$ the estimated value of the emitted frequency of the target, $(\dot{\xi}_o(k),\dot{\eta}_o(k))$ the components of the ownship velocity, also assumed perfectly known, and *c* the sound velocity set in our simulations to 1500 *m/s*. The corresponding covariance matrix is

$$R=\begin{bmatrix}\sigma_\beta^2 & 0\\ 0 & \sigma_{f_e}^2\end{bmatrix} \tag{3.37}$$

where σ_{f_e} is the standard deviation of the measured frequency. Here, the emitted frequency of the target f_e, which we assume nearly constant (i.e. following a random walk model) during the scenario and starting with 300 *Hz*, is unknown. Hence, the state vector has to be augmented and (3.24) is replaced for the first model by

$$x(k)=\begin{bmatrix}\xi(k) & \eta(k) & \dot{\xi}(k) & \dot{\eta}(k) & f_e(k)\end{bmatrix}' \tag{3.38}$$

Thus, the NCV transition model (3.26) is modified as

$$F_{1b}=\begin{bmatrix}F_1 & 0\\ 0 & 1\end{bmatrix} \tag{3.39}$$

and the covariance matrix (3.27) as

$$Q_{1b}=\begin{bmatrix}Q_1 & 0\\ 0 & q_{f_e}T\end{bmatrix} \tag{3.40}$$

with q_{f_e} the process noise PSD for the frequency. For mode 2, (3.28) is also now replaced by

$$x(k)=\begin{bmatrix}\xi(k) & \eta(k) & \dot{\xi}(k) & \dot{\eta}(k) & f_e(k) & \omega(k)\end{bmatrix}' \tag{3.41}$$

and state prediction (3.30) is suitably modified as

Authorized licensed use limited to: Purdue University. Downloaded on September 15,2025 at 23:34:05 UTC from IEEE Xplore. Restrictions apply.

$$f_2(x(k))=\begin{cases}\xi(k)+T\dot{\xi}(k)+\dfrac{T^2}{2}\omega(k)\dot{\eta}(k)\\ \eta(k)+T\dot{\eta}(k)-\dfrac{T^2}{2}\omega(k)\dot{\xi}(k)\\ \dot{\xi}(k)+T\omega(k)\dot{\eta}(k)-\dfrac{T^2}{2}\omega^2(k)\dot{\xi}(k)\\ \dot{\eta}(k)-T\omega(k)\dot{\xi}(k)-\dfrac{T^2}{2}\omega^2(k)\dot{\eta}(k)\\ f_e(k)\\ \omega(k)\end{cases} \tag{3.42}$$

with the corresponding process noise covariance matrix

$$Q_{2b}=\begin{bmatrix} q_2\begin{bmatrix} T^3/3 & 0 & T^2/2 & 0\\ 0 & T^3/3 & 0 & T^2/2\\ T^2/2 & 0 & T & 0\\ 0 & T^2/2 & 0 & T\end{bmatrix} & \begin{matrix}0_{4\times1}\\ \\ \end{matrix} & \begin{matrix}0_{4\times1}\\ \\ \end{matrix}\\ \begin{matrix}0_{1\times4}\\ 0_{1\times4}\end{matrix} & & \begin{matrix}q_{f_e}T & 0\\ 0 & q_\omega T\end{matrix}\end{bmatrix} \tag{3.43}$$

Filter initialization

In the case of bearing only measurements, we use an a priori distance d_0 with standard deviation σ_{d0} and the first bearing measurement β_0 with its standard deviation σ_β to set the position components of x_0 and its covariance matrix P_0. We then carry out the Unbiased Transformation (UT) ([3]) from polar coordinates (d_0,β_0) with covariance

$$\begin{bmatrix}\sigma_{d0}^2 & 0\\ 0 & 9\sigma_\beta^2\end{bmatrix} \tag{3.44}$$

to CC and obtain (ξ_0,η_0) and its corresponding covariance matrix given by the UT

$$\begin{bmatrix}\sigma_\xi^2 & \sigma_{\xi\eta}^2\\ \sigma_{\xi\eta}^2 & \sigma_\eta^2\end{bmatrix} \tag{3.45}$$

On the other hand, the velocity component estimates of the target are set to zero with initial variances $\sigma_{\dot{\xi}}^2$ and $\sigma_{\dot{\eta}}^2$. This amounts to starting the first mode-matched filter with the initial state vector given by

$$x_{10}=\begin{bmatrix}\xi_0 & \eta_0 & 0 & 0\end{bmatrix}' \tag{3.46}$$

with covariance matrix

$$P_{10}=\begin{bmatrix}\sigma_\xi^2 & \sigma_{\xi\eta}^2 & 0 & 0\\ \sigma_{\xi\eta}^2 & \sigma_\eta^2 & 0 & 0\\ 0 & 0 & \sigma_{\dot{\xi}}^2 & 0\\ 0 & 0 & 0 & \sigma_{\dot{\eta}}^2\end{bmatrix} \tag{3.47}$$

For mode 2, we simply initialize the turn rate with 0 and (3.46) is augmented as

$$x_{20}=\begin{bmatrix}\xi_0 & \eta_0 & 0 & 0 & 0\end{bmatrix}' \tag{3.48}$$

with initial covariance matrix given by

$$P_{20}=\begin{bmatrix}\sigma_\xi^2 & \sigma_{\xi\eta}^2 & 0 & 0 & 0\\ \sigma_{\xi\eta}^2 & \sigma_\eta^2 & 0 & 0 & 0\\ 0 & 0 & \sigma_{\dot{\xi}}^2 & 0 & 0\\ 0 & 0 & 0 & \sigma_{\dot{\eta}}^2 & 0\\ 0 & 0 & 0 & 0 & \sigma_{\omega0}^2\end{bmatrix} \tag{3.49}$$

In the case of active measurement, the a priori distance is replaced by the first measured distance, and the a priori standard deviation σ_{d0} in (3.44) is replaced by the distance measurement noise standard deviation σ_d multiplied by 3. In the case of passive measurement with Doppler, (3.46) for mode 1 is replaced by

$$x_{10}=\begin{bmatrix}\xi_0 & \eta_0 & 0 & 0 & f_m\end{bmatrix}' \tag{3.50}$$

with f_m the first measured frequency, and (3.47) suitably modified as

$$P_{10}=\begin{bmatrix}\sigma_\xi^2 & \sigma_{\xi\eta}^2 & 0 & 0 & 0\\ \sigma_{\xi\eta}^2 & \sigma_\eta^2 & 0 & 0 & 0\\ 0 & 0 & \sigma_{\dot{\xi}}^2 & 0 & 0\\ 0 & 0 & 0 & \sigma_{\dot{\eta}}^2 & 0\\ 0 & 0 & 0 & 0 & 9\sigma_f^2\end{bmatrix} \tag{3.51}$$

In the same way, for the second mode-matched filter, (3.48) is augmented as

$$x_{20}=\begin{bmatrix}\xi_0 & \eta_0 & 0 & 0 & f_m & 0\end{bmatrix}' \tag{3.52}$$

and (3.51) is now replaced by

Authorized licensed use limited to: Purdue University. Downloaded on September 15,2025 at 23:34:05 UTC from IEEE Xplore. Restrictions apply.

$$P_{20} = \begin{bmatrix} \sigma_{\xi}^2 & \sigma_{\xi\eta}^2 & 0 & 0 & 0 & 0 \\ \sigma_{\xi\eta}^2 & \sigma_{\eta}^2 & 0 & 0 & 0 & 0 \\ 0 & 0 & \sigma_{\dot{\xi}}^2 & 0 & 0 & 0 \\ 0 & 0 & 0 & \sigma_{\dot{\eta}}^2 & 0 & 0 \\ 0 & 0 & 0 & 0 & 9\sigma_f^2 & 0 \\ 0 & 0 & 0 & 0 & 0 & \sigma_{\omega 0}^2 \end{bmatrix} \quad (3.53)$$

4.2 Comparative study with IMM

In the following results, where all MC simulations are carried out with 1000 runs, we compare the IMM filter with the GMIMM. Since we have non linear dynamics, we use the UKF approximation to compute the conditional densities ([5]) with parameters $\alpha = 0.01$, $\beta = 2$. Since mode 2 has an extra state as compared to mode 1, namely the angular velocity ω, the mixing is done with the assumption that for mode 1 it is initialized with zero and with a small variance of $1\,10^{-10}\ (rad/s)^2/s$: this is requested in the UKF extrapolation step where a Cholesky decomposition of the covariance matrix is needed. If an EKF is used, it can bet set to zero.

Scenario

The target starts at (12 km, 0 km) with velocity 8 knots (4.12 m/s) and heading angle 225°. At *t* = 30', it performs a clockwise 110° coordinated turn until *t* = 35' and at *t* = 65', it performs a 110° counter clockwise coordinated turn until *t* = 70' both with turn rate ω = 0.375°/s. The own-ship starts at (0 km, 4.5 km) with velocity 10 knots (5.15 m/s) and heading angle 180°. At times *t* = 10', 45' and 75', it performs different coordinated turns. Fig.5 is a plot of the considered scenario where the small squares indicate the initial positions.

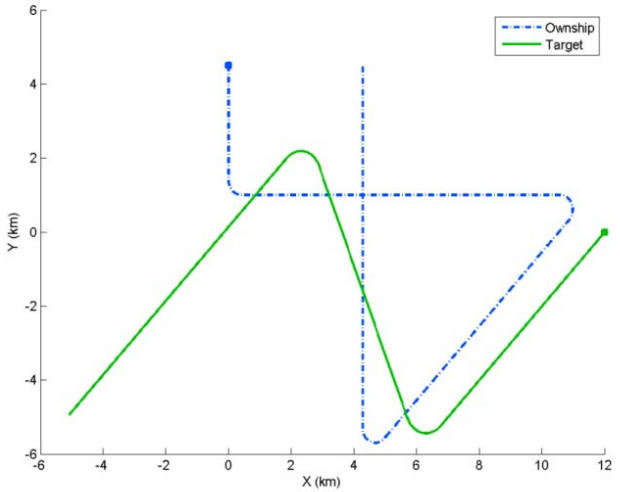

Fig.5 – Scenario

Parameter settings

The sampling rate is set to $T = 12\ s$, a typical value in sonar applications.

The process noise levels are given by

- $q_1 = 1\,10^{-5}\ m^2/s^3$, $q_2 = 2\,10^{-3}\ m^2/s^3$,
- $q_{fe} = 1\,10^{-6}\ Hz^2/s = 1\,10^{-6}\ 1/s^3$,
- $q_{\omega} = 7.5\,10^{-7}\ (rad/s)^2/s = 7.5\,10^{-7}\ rad^2/s^3$

The measurements are simulated with the exact geometry corrupted by an additive white zero mean Gaussian noise with

- $\sigma_{\beta} = 1°$ for the bearing measurements,
- $\sigma_d = 20\ m$ for the range measurements,
- $\sigma_{fe} = 0.03\ Hz$ for the Doppler measurements.

For the state and covariance initialization,

- the a priori range d_0 is set to 18 km, with $\sigma_{d0} = 4\ km$,
- the initial velocities standard deviations are set to $\sigma_{\dot{\xi}} = \sigma_{\dot{\eta}} = 10\ m/s$,
- the initial standard deviation for the turn rate is $\sigma_{\omega 0} = 0.1\ rad/s$.

Finally, the initial mode probabilities are

- $\mu_0 = [0.9 \quad 0.1]'$

and the TPM is set to

- $\Pi = \begin{bmatrix} 0.98 & 0.02 \\ 0.02 & 0.98 \end{bmatrix}$

The six following figures (Fig.6 to Fig11) compare the performances of the IMM and the GMIMM with *r* = 1 (which corresponds to the illustration of Fig.3), i.e. with keeping only one (the most probable) Gaussian in each mode, the remaining ones being combined into a single Gaussian, for the three measurement configurations. In the BOT case, the improvement is already significant compared to the IMM and this both during the nominal periods as well as during the maneuvering ones. In the bearing and Doppler case, the improvement is very limited. In the active case, the benefit over the IMM occurs only during the uniform periods, especially at the end of the scenario.

Then, we study the influence of the parameter *r* on the performance, and we expect that it improves as *r* increases. The six next following figures (Fig.12 to Fig17) plot the results obtained on the three cases for *r* = 1, 5, 10 & 20. In the BOT case, the performance clearly improves as the order of the filter increases and the RMS position error is again divided by two with *r* = 10 at the end of the scenario. In the bearing and Doppler case, the same tendency can be observed, but it is less contrasted. The difference here is that we have to use a higher order *r* to obtain a significant improvement.

Authorized licensed use limited to: Purdue University. Downloaded on September 15,2025 at 23:34:05 UTC from IEEE Xplore. Restrictions apply.

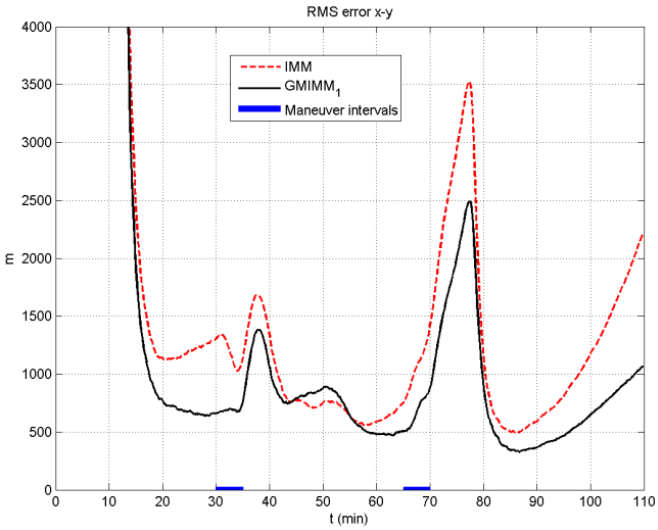

Fig.6 – Position error, BOT case

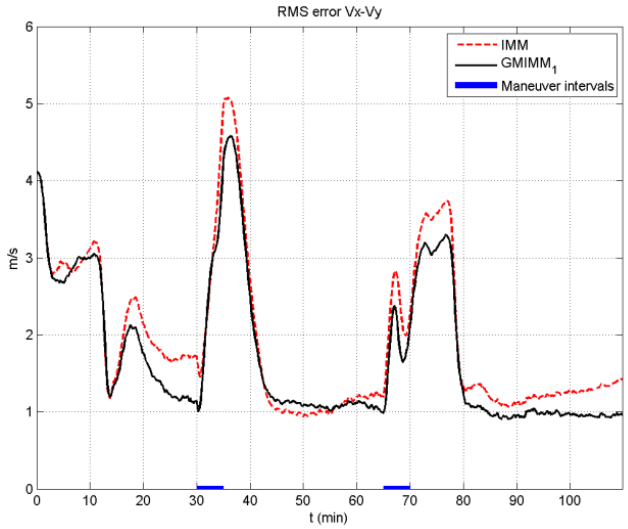

Fig.7 – Velocity error, BOT case

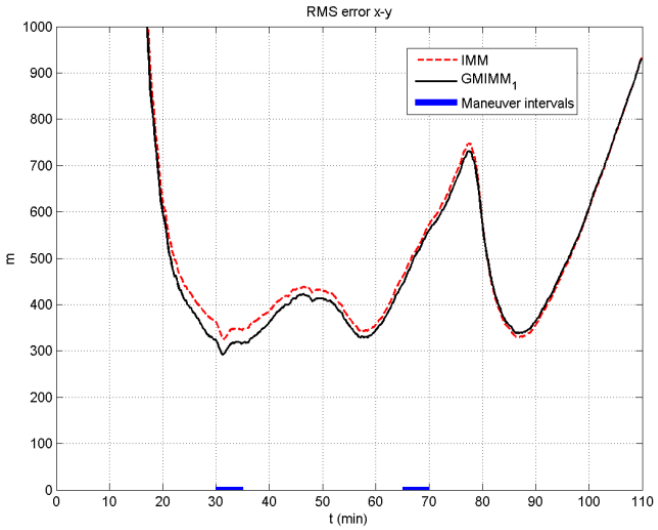

Fig.8 – Position error, bearing and Doppler case

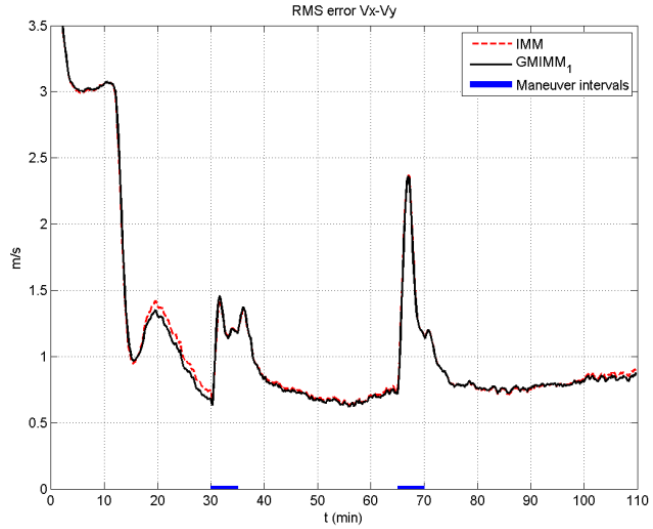

Fig.9 – Velocity error, bearing and Doppler case

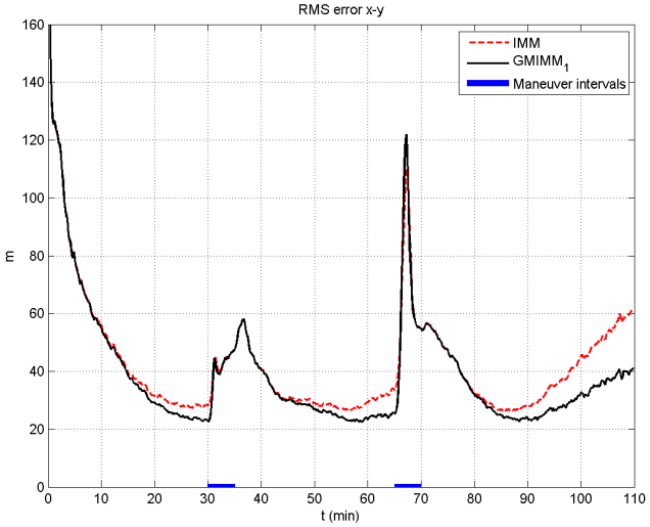

Fig.10 – Position error, bearing and distance case

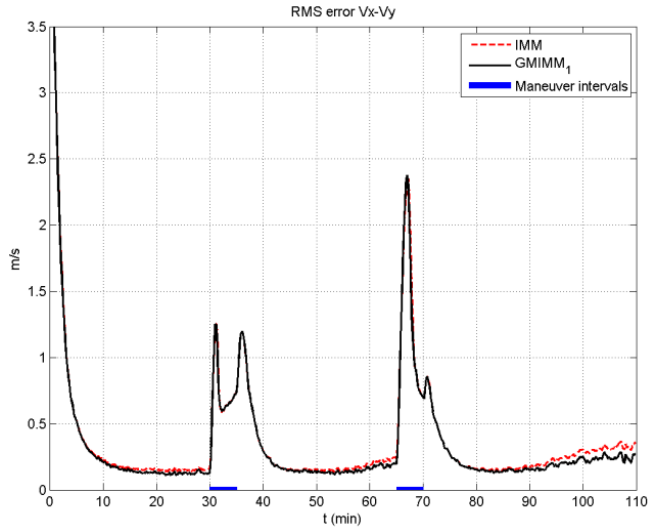

Fig.11 – Velocity error, bearing and distance case

Authorized licensed use limited to: Purdue University. Downloaded on September 15,2025 at 23:34:05 UTC from IEEE Xplore. Restrictions apply.

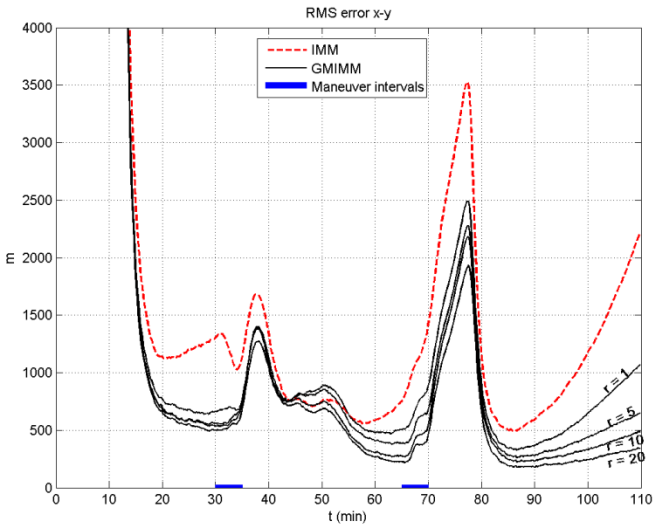

Fig.12 – Position error, BOT case

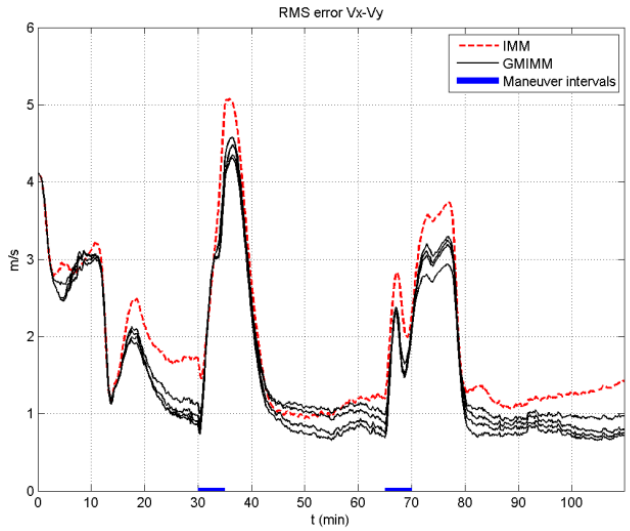

Fig.13 – Velocity error, BOT case

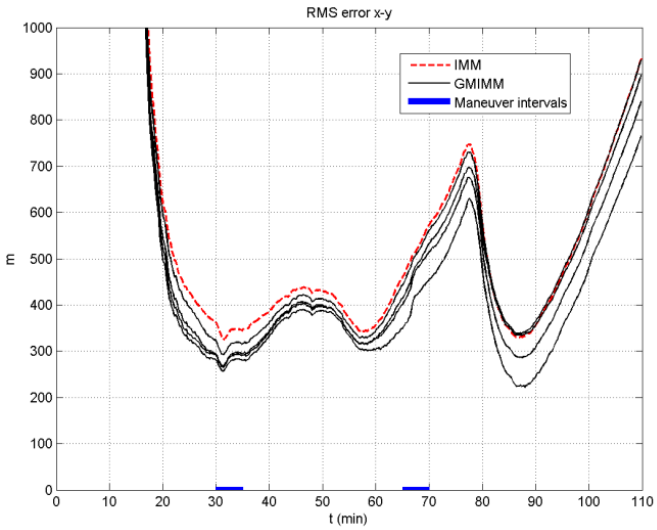

Fig.14 – Position error, bearing and Doppler case

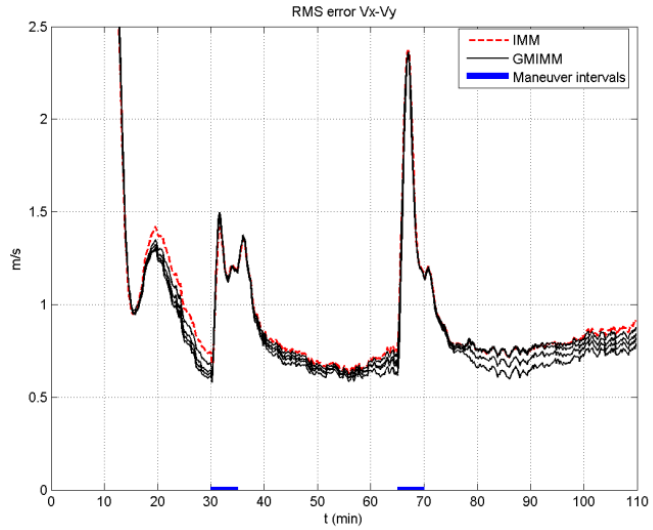

Fig.15 – Velocity error, bearing and Doppler case

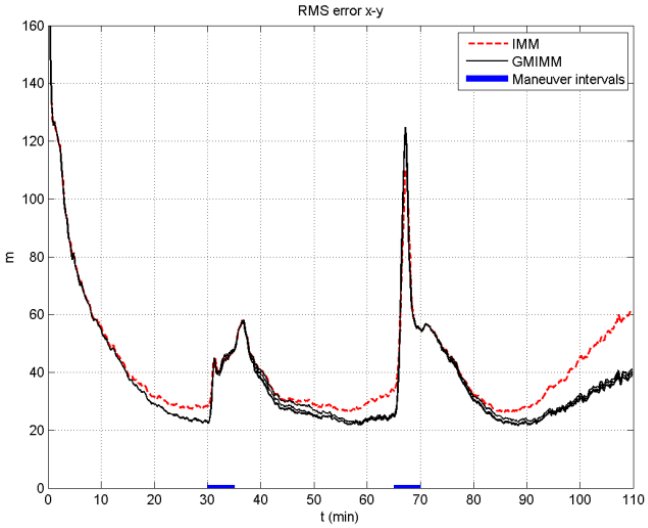

Fig.16 – Position error, bearing and distance case

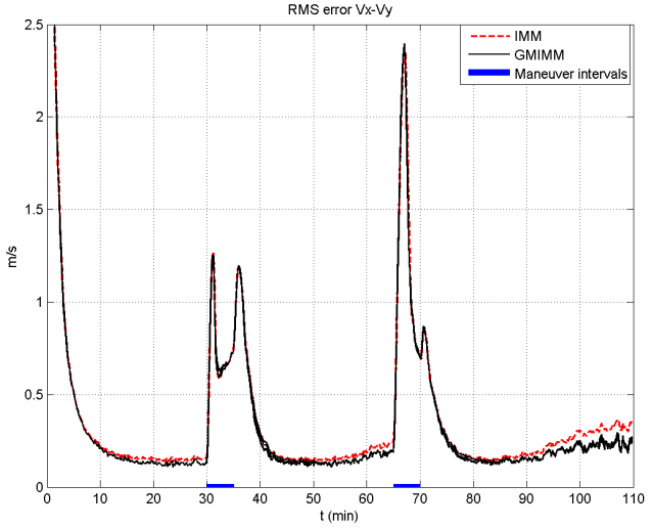

Fig.17 – Velocity error, bearing and distance case

Authorized licensed use limited to: Purdue University. Downloaded on September 15,2025 at 23:34:05 UTC from IEEE Xplore. Restrictions apply.

In the active case (Fig.16 & 17), on the contrary, no noticeable improvement (second order magnitude) is obtained when increasing the order of the filter and the best compromise in this latter case is thus obtained with $r = 1$.

5. CONCLUSION

We have studied a new approach for the maneuvering target tracking problem, the Gaussian Mixture based IMM (GMIMM) filter of order *r*, where the IMM filter is obtained as a particular case with the lowest order ($r = 0$) of this approach, mixing all elements into a single Gaussian in each mode and at the beginning of each cycle.

We have compared this new approach with the IMM filter in a sonar application with three measurement configurations, one active and two passive. In the active case, the improvement of the new approach is limited : no improvement (or second order) with an increasing *r* and slight improvement over IMM with $r = 1$ (only during uniform periods). The best performance/complexity compromise is thus obtained in this case with $r = 1$. In the passive case, on the contrary, the improvement of the new approach increases with the order *r*, but slower in the bearing and Doppler case than in the BOT case. In this latter case, contrary to the bearing and Doppler case, the improvement over the IMM filter is already significant with $r = 1$. The main advantage of this new approach, in the passive case, is that we can control the performance improvement as the order of the filter *r* increases. Of course the computational time also increases, but *linearly* with the order thanks to the mixing/reduction phase before the filtering.

These results have been obtained on a particular scenario in a sonar context and other simulations in the same and in another context (airborne scenario in jamming conditions like in [4]) have to be carried out in order to confirm these first results.

REFERENCES

[1] S. Arulampalam, S. Maskell, N. Gordon and T. Clapp, "A Tutorial on Particle Filters for Online Nonlinear/Non-Gaussian Bayesian Tracking", *IEEE Trans. on Signal Proc.*, 50 (2), Feb. 2002.

[2] H. A. P. Blom, Y. Bar-Shalom, "The interacting multiple model algorithm for systems with Markovian switching coefficients", *IEEE Transactions on Automatic Control*, **33** , pp. 780-783, Aug. 1988.

[3] Y. Bar-Shalom, X.R Li, T. Kirubarajan, "Estimation with Applications to Tracking and Navigation", *Wiley*, 2001.

[4] B. Ristic, S.M. Arulampalam, "Tracking a manoeuvring target using angle-only measurements: algorithms and performance", *Signal Processing*, 83, pp. 1223-1238, 2003.

[5] E. A.Wan, R. Van der Merwe, "The Unscented Kalman Filter for Nonlinear Estimation", in *Proc. AS-SPCC Symposium 2000*, Lake Louise, Alberta, Canada, 1-4 Oct. 2000.

BIOGRAPHIES

Dann Laneuville *received the "diplôme d'ingénieur" from Ecole Supérieure d'Electricité (a.k.a. Supélec) in 1987 and a Ph.D. in automatic and signal processing from the Paris XI Orsay University in 1998. He is currently with DCNS as a senior algorithms expert in Information and Surveillance Systems. Before joining DCNS in 2003, he has been with EADS for ten years and with MBDA for five years. His area of interest are Multitarget Tracking, Data Fusion, Target Motion Analysis and more recently Image Processing.*

Yaakov BarShalom *was born on May 11, 1941. He received the B.S. and M.S. degrees from the Technion, Israel Institute of Technology, in 1963 and 1967 and the Ph.D. degree from Princeton University in 1970, all in electrical engineering. From 1970 to 1976 he was with Systems Control, Inc., Palo Alto, California. Currently he is Board of Trustees Distinguished Professor in the Dept. of Electrical and Computer Engineering and Marianne E. Klewin Professor in Engineering at the University of Connecticut. He is also Director of the ESP (Estimation and Signal Processing) Lab. His current research interests are in estimation theory, target tracking and data fusion. He has published over 400 papers and book chapters in these areas and in stochastic adaptive control. He coauthored the monograph Tracking and Data Association (Academic Press, 1988), the graduate texts Estimation and Tracking: Principles, Techniques and Software (Artech House, 1993), Estimation with Applications to Tracking and Navigation: Algorithms and Software for Information Extraction (Wiley, 2001), the advanced graduate texts MultitargetMultisensor Tracking: Principles and Techniques (YBS Publishing, 1995), Tracking and Data Fusion (YBS Publishing, 2011), and edited the books MultitargetMultisensor Tracking: Applications and Advances (Artech House, Vol. I, 1990; Vol. II, 1992; Vol. III, 2000). He has been elected Fellow of IEEE for "contributions to the theory of stochastic systems and of multi target tracking". He has been consulting to numerous companies and government agencies, and originated the series of MultitargetMultisensor Tracking short courses offered via UCLA Extension, at Government Laboratories, private companies and overseas. During 1976*

Authorized licensed use limited to: Purdue University. Downloaded on September 15,2025 at 23:34:05 UTC from IEEE Xplore. Restrictions apply.

and 1977 he served as Associate Editor of the IEEE Transactions on Automatic Control and from 1978 to 1981 as Associate Editor of Automatica. He was Program Chairman of the 1982 American Control Conference, General Chairman of the 1985 ACC, and CoChairman of the 1989 IEEE International Conference on Control and Applications. During 1983--87 he served as Chairman of the Conference Activities Board of the IEEE Control Systems Society and during 1987--89 was a member of the Board of Governors of the IEEE CSS. He was a member of the Board of Directors of the International Society of Information Fusion (1999--2004) and served as General Chairman of FUSION 2000, President of ISIF in 2000 and 2002 and Vice President for Publications in 2004-11. In 1987 he received the IEEE CSS Distinguished Member Award. Since 1995 he is a Distinguished Lecturer of the IEEE AESS and has given numerous keynote addresses at major national and international conferences. He is co-recipient of the M. Barry Carlton Award for the best paper in the IEEE Transactions on Aerospace and Electronic Systems in 1995 and 2000 and recipient of the 1998 University of Connecticut AAUP Excellence Award for Research. In 2002 he received the J. Mignona Data Fusion Award from the DoD JDL Data Fusion Group. He is a member of the Connecticut Academy of Science and Engineering. In 2008 he was awarded the IEEE Dennis J. Picard Medal for Radar Technologies and Applications.

Authorized licensed use limited to: Purdue University. Downloaded on September 15,2025 at 23:34:05 UTC from IEEE Xplore. Restrictions apply.

APPENDIX A
GMIMM Block diagram

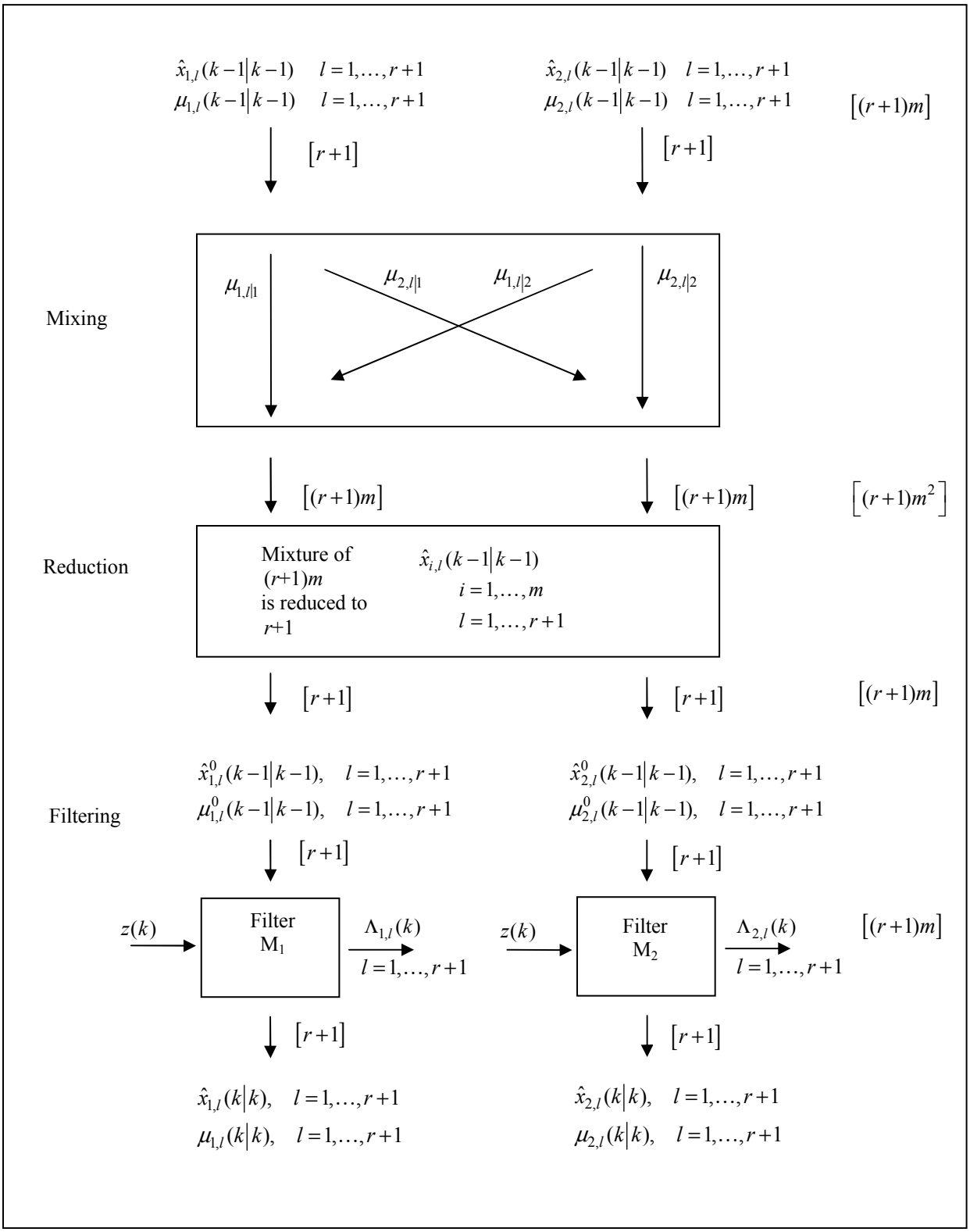

Fig.4 – GMIMM for $m = 2$ modes and r hypotheses. The terms in brackets indicate the cardinalities of the sets of estimates and covariances (the latter not shown)

Authorized licensed use limited to: Purdue University. Downloaded on September 15,2025 at 23:34:05 UTC from IEEE Xplore. Restrictions apply.